

Working title:

Mirage effect in multilayers

An experimental and theoretical approach of the photothermal deflection effect in multilayered semiconductor samples to obtain the thermal diffusivity.

Martijn Heck
id: 414527
m.j.r.heck@stud.tue.nl

Summary

The Mirage effect is a special form of photothermal material probing. The heat diffusion through a sample is studied in an indirect way. A sample is illuminated with a modulated laser pump beam. The heat waves that result from this modulated heating are detected by a laser probe beam that passes through the surrounding coupling fluid. As the rising temperature induces a gradient in the index of refraction of the coupling fluid, the probe beam is deflected. By recording the phase of the deflection the thermal diffusivity of the sample material can be obtained.

In this report the Mirage effect in a multilayer semiconductor sample is reviewed. To obtain the thermal diffusivity of an individual layer, an experimental approach as well as a theoretical approach is chosen.

For the experimental technique a setup is build. First the setup is utilized to get the thermal diffusivity of bulk samples, like GaAs. In this way the setup is tested and reviewed. Secondly a sample composed of two epitaxial layers is reviewed. The experimental results can not be interpreted with the existing theory.

To interpret the experimental results the existing theory to obtain the thermal diffusivity is expanded to a two-layered sample. The analytical equations have to be calculated numerically. To this end a computer program is developed. This program is tested on mathematical and physical correctness.

Finally the theoretical and the experimental approach are compared. Inaccuracies in the experimental part as well as limited practical use of the theoretical model make the linking together of both approaches in this report impossible.

Nevertheless both approaches are useful in their own way and offer the opportunity to be a step in the eventual synthesis of theory and experiment.

Contents

1. Introduction	?
2. Theory of the Mirage effect	?
2.1. Parameters involved in the Mirage effect	?
2.2. Temperature distribution in a medium	?
2.3. Mirage deflection of the probe beam	?
3. Experimental setup for Mirage measurements	?
3.1. Description of the individual parts	?
3.2. Operation of the setup	?
4. Experimental results	?
4.1. Thermal diffusivity of GaAs and InP	?
4.2. Specific experimental problems concerning the Mirage effect.....	?
4.2.1. <i>Tilted sample</i>	?
4.2.2. <i>Irregularities on the sample surface</i>	?
4.2.3. <i>Other method for determining the thermal diffusivity</i>	?
4.3. Experimental results with 2-layered samples.....	?
5. Theoretical model	?
5.1. Theory for a two-layered sample	?
5.2. Model	?
5.3. Evaluation of the Model.....	?
5.3.1. <i>Accuracy of the model</i>	?
5.3.2. <i>Analytical correctness of the model</i>	?
5.3.3. <i>Physical correctness of the model</i>	?
5.4. Two layers: interpretations.....	?
6. Discussion	?
6.1. Setup review.....	?
6.1.1. <i>Vibrations</i>	?
6.1.2. <i>Fibre-based detector</i>	?
6.2. Experiments versus model	?
References	?
Appendices	?
A. Temperature equations	?
B. Matlab source code.....	?
Acknowledgements	?

1. Introduction

Photothermal (PT) generation is a result of the heating of a sample due to absorption of electromagnetic radiation. This phenomenon has an enormously wide range of applications, both in the field of physics, as in fields like chemistry and biology. In general this effect can be used for two kinds of applications. The first application is one in which the material under study will undergo a change. When the material is converted in a useful one, the process is called PT processing. If the material is rendered useless, it is called PT destruction. The second application is one in which the material will not be modified. This is called PT material probing. A good overview of this application is given in [1]. Figure 1 gives an overview of the different effects that occur with PT material probing.

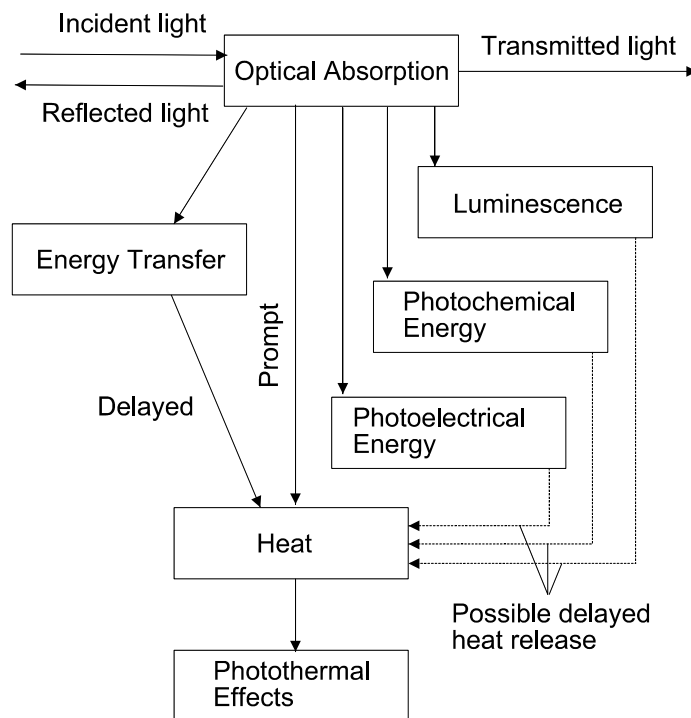


fig. 1: Indication of the possible consequences of optical absorption. This results in 'prompt' or 'delayed' heat production in competition with other de-excitation channels [1].

Modulated PT heating of a material will cause several effects, both direct, in the material itself, as indirect in the surrounding material, called the coupling fluid. This effect is called indirect because the coupling fluid is not (significantly) heated by the modulated PT source, but indirect by the material. Of course many effects can occur at the same time. Figure 2 gives a survey of some of the possible effects.

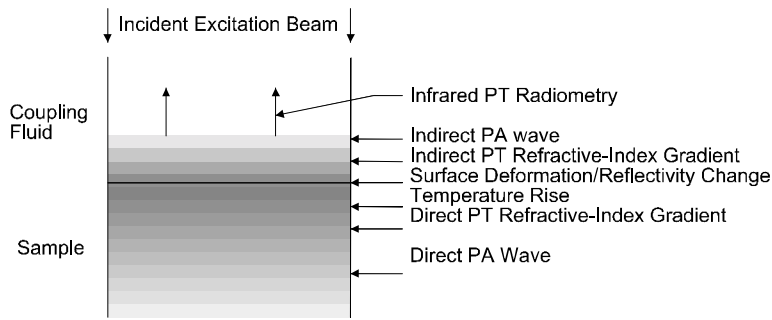


fig. 2: Common photothermal effects produced by modulated optical absorption in a sample. The shades of grey are a measure for the local temperature increase. PT heating leads to both PT effects as photoacoustic (PA) effects [1].

In this report the change in the refractive index, also called refractive index gradient (RIG), as a result of applied modulated heating is considered. RIG occurs both direct in the sample material as indirect in the coupling fluid. Generally this effect can be used in three ways: parallel probe-beam refraction (PBR), perpendicular PBR in the sample and PBR outside the sample, also called the mirage effect (see figure 3).

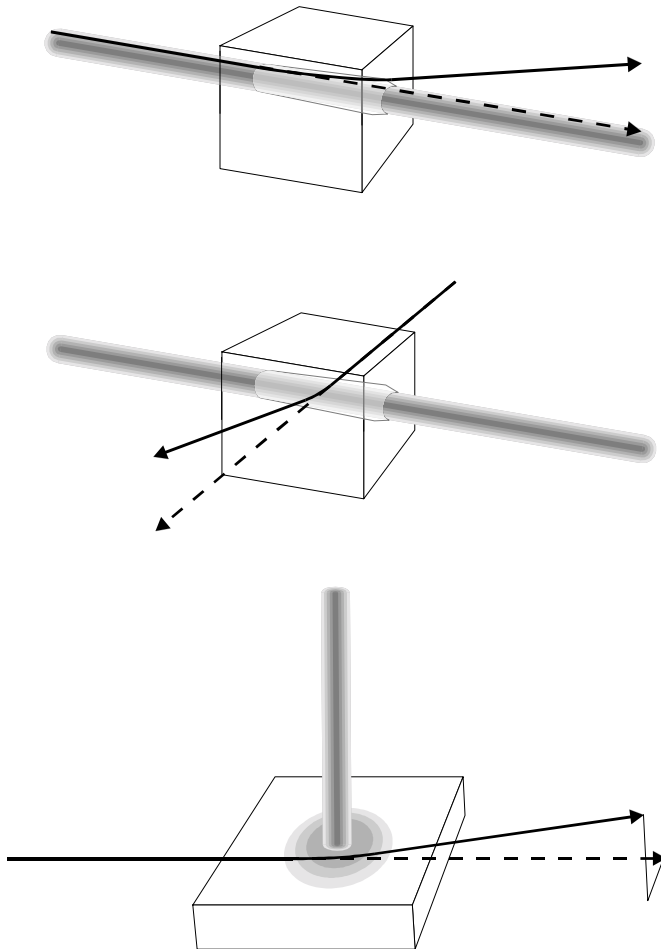


fig. 3: Different setups for PBR measurements: a) parallel PBR, b) perpendicular PBR in the sample and c) PBR outside the sample [1].

Although different in geometrical setup the three techniques are based on a common principle. A high power (laser) pump beam heats the sample periodically. This results in a change in the refractive index in the material. As a result a low power (laser) probing beam is deflected when passing the gradient in the refractive index.

The main target of this research project is to gain insight in the thermodynamic behavior of multilayered samples under the periodic heating of the PBR setup in general and to derive the thermal diffusivity coefficient of the individual layers specifically.

As the samples under study (multilayered semiconductors) are opaque for the used lasers this report focuses on the PBR outside sample or mirage effect, which was introduced by Boccara et al. [2]. By measuring the time evolution of the thermal RIG the thermal diffusivity can be calculated.

The report is structured in the following way.

Chapter 2 provides the theory and the basic equations to describe the signal as obtained with the mirage effect and to calculate the thermal diffusivity.

Chapter 3 describes the experimental setup used to do the measurements. The individual components are reviewed.

Chapter 4 describes the experimental results obtained with the used setup.

Chapter 5 provides a model for interpretation of the mirage deflection signal of a two-layered sample. The fundamentals of the model are examined. The model is used to gain insight in the thermodynamic behavior of the sample as a result of varying the different input parameters.

Both parameters related to the setup as to the sample are reviewed.

Chapter 6 concludes the treatment of the topic with a discussion of the results, the used setup and the used model.

2. Theory of the Mirage effect

This chapter describes the theory concerning the mirage effect. In 2.1 an overview is given of the relevant parameters as used in the mirage setup as well as their definitions. Here also an overview is given of the used setup and geometry.

The general theory about the heat distribution in and outside a bulk sample is given in 2.2. In 2.3 the theory concerning the deflection of the probe beam is summarized. This overview gives the methods to obtain the relevant data out of the deflection signal.

2.1. Parameters involved in the Mirage effect

As the literature is very inconsistent in assigning symbols to the relevant physical parameters, a survey is given of the parameters used throughout this report and their definition. For clarity and for explaining the meaning of the different parameters a schematic view of the setup for measurements with the Mirage effect is given in figure 2.1.

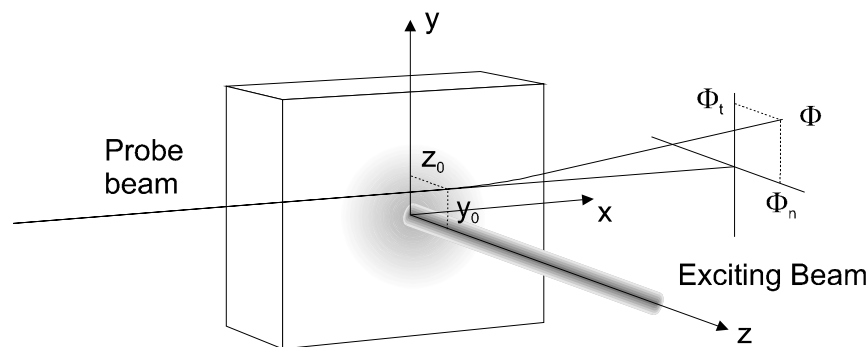


fig. 2.1: Geometry of the mirage deflection; transverse and normal deflection are not scaled

The symbols and definitions used in this report are as follows:

Symbol	Meaning	Units
α	Optical absorption coefficient	m^{-1}
C_p	Specific heat	$\text{J}\cdot\text{kg}^{-1}\cdot\text{K}^{-1}$
ρ	Density	$\text{kg}\cdot\text{m}^{-3}$
D	Thermal diffusivity	$\text{m}^2\cdot\text{s}^{-1}$
k	Thermal conductivity	$\text{W}\cdot\text{m}^{-1}\cdot\text{K}^{-1}$
T	Temperature	K
y_0	Transverse offset pump - probe	m
z_0	Height probe beam above sample surface	m
$\omega=2\pi f$	Modulation frequency pump beam	s^{-1}
a	Pump beam radius at $1/e$ of (Gaussian) intensity	m
b	Probe beam radius at $1/e$ of (Gaussian) intensity	m

2.2. Temperature distribution in a medium

A good survey of the temperature distribution in a medium is given by Salazar et al. [3]. The hydrodynamic and thermodynamic equations that describe the temperature field in a medium are:

$$\frac{d\rho}{dt} + \rho \nabla u = 0, \quad (2.1)$$

$$\rho \frac{du}{dt} = -\nabla P + F, \quad (2.2)$$

$$\rho \frac{de}{dt} = -P \cdot \nabla u - \nabla q + \chi + Q, \quad (2.3)$$

$$\rho = \rho(P, T), \quad (2.4)$$

in which ρ is the density, P the pressure, T the temperature, u the velocity, F the forces acting on a unit volume of fluid, e the internal energy per unit mass, q the macroscopic heat flux, $P \cdot \nabla u$ the pressure force work, χ the viscous dissipation term and Q the heat per unit volume due to sources.

The following assumptions are made:

- Convective and radiative heat transfer effects can be neglected ($q = -k \nabla T$);
- Steady and frictionless conditions ($u=0, \chi=0$);
- The sample is thermally and elastically isotropic;
- The contribution from the acoustic wave to the thermal field is omitted [4].

This leads to the heat diffusion equation:

$$\nabla^2 T - \frac{1}{D} \frac{\partial T}{\partial t} + \frac{Q}{k} = 0, \quad (2.4)$$

with the thermal diffusivity D

$$D = k / \rho C_p. \quad (2.5)$$

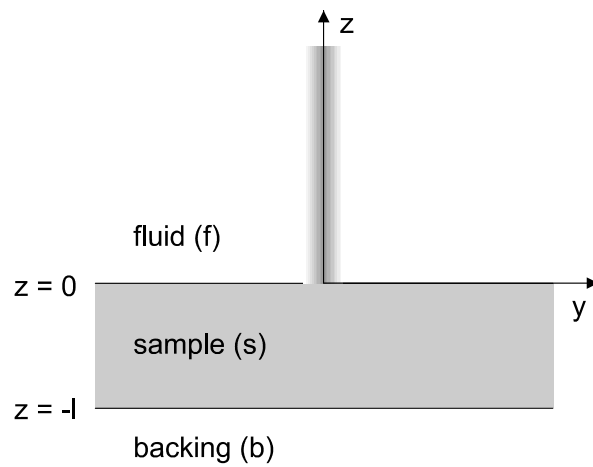


fig. 2.2: Geometry for the thermal field evaluation

For a heterogeneous, bulk sample under study, with a geometry as given in figure 2.2, the following set of equations is derived for the time-dependent (ac) component of the temperature field, using (2.4):

$$\nabla^2 T_f - \frac{1}{D_f} \frac{\partial T_f}{\partial t} = 0, \quad (2.6)$$

$$\nabla^2 T_s - \frac{1}{D_s} \frac{\partial T_s}{\partial t} = -\frac{Q(r,t)}{k_s}, \quad (2.7)$$

$$\nabla^2 T_b - \frac{1}{D_b} \frac{\partial T_b}{\partial t} = 0 \quad (2.8)$$

Here the assumption is made that the (coupling) fluid and the backing are nonabsorbent to the modulated source (pump beam), so $\alpha_f, \alpha_b = 0$. As a result the heat Q due to sources equals 0. Also the assumption is made that the dimensions extend to infinity (both the surface plane in (x,y)-directions as the fluid and backing in the perpendicular z-direction).

For this set, the following boundary conditions apply:

$$\begin{aligned} T_f(z=0) &= T_s(z=0) \\ T_s(z=-\ell) &= T_b(z=-\ell), \end{aligned} \quad (2.9)$$

the temperature continuity at the sample surfaces ($z=0$ and $z=-\ell$), and

$$\begin{aligned} k_f \left. \frac{\partial T_f}{\partial z} \right|_{z=0} &= k_s \left. \frac{\partial T_s}{\partial z} \right|_{z=0} \\ k_s \left. \frac{\partial T_s}{\partial z} \right|_{z=-\ell} &= k_b \left. \frac{\partial T_b}{\partial z} \right|_{z=-\ell}, \end{aligned} \quad (2.10)$$

the heat-flow continuity at the sample surfaces.

The source Q used in the experiments is a modulated laser beam (pump beam). Two assumptions are made for the source. First a Gaussian beam profile is assumed for the laser beam. Second a light absorption to heat conversion efficiency by nonradiative de-excitation processes is assumed to be one. This means that no absorbed energy will be lost in the form of radiation. The distribution of the source Q is both dependent on position as on time, so $Q=Q(r,t)$.

With the given assumptions Q can be expressed in cylindrical coordinates as

$$Q(r,t) = \left(\frac{P_0 \alpha}{2\pi a^2} \right) \exp(\alpha z) \exp\left(\frac{-r^2}{a^2} \right) \exp(i\omega t), \quad (2.11)$$

with P_0 the exciting beam power.

The set of equations defined by (2.6)-(2.10) can be solved analytically [3] to obtain the temperature distribution. The solutions are given in Appendix A. Here only the equation for the temperature distribution in the coupling fluid is given, as this is used in the experiments based on the mirage effect:

$$T_f(r, z, t) = \frac{1}{2} \int_0^{\infty} \delta J_0(\delta r) E(\delta) \exp(-\beta_f z) \exp(i\omega t) d\delta, \quad (2.12)$$

where $\beta_f^2 = \delta^2 + (i\omega/D_f)$ and with the function $E(\delta)$ given by:

$$E(\delta) = \frac{P_0}{2\pi k_s} \frac{p}{\beta_s(1-p^2)} \exp\left(-\frac{(\delta\alpha)^2}{4}\right) \times \left(\frac{(1+b)(1-p)\exp(\beta_s\ell) - (1-b)(1+p)\exp(-\beta_s\ell) - 2(b-p)\exp(-\alpha\ell)}{(1+g)(1+b)\exp(\beta_s\ell) - (1-g)(1-b)\exp(-\beta_s\ell)} \right) \quad (2.13)$$

with $g = k_f\beta_f/k_s\beta_s$, $b = k_b\beta_b/k_s\beta_s$ and $p = \alpha/\beta_s$.

2.3. Mirage deflection of the probe beam

As seen in figure 2.1, the probe beam travels parallel to the sample surface through the coupling fluid. Resulting from the refractive index gradient the probe beam gets deflected. This deflection is given by [5]:

$$\varphi = -\frac{1}{n} \frac{dn}{dT} \int_{-\infty}^{\infty} \nabla T_f \times dl, \quad (2.12)$$

with n the fluid refractive index and l the optical path length. This total deflection can be decomposed in two components, one normal to the sample surface, φ_n , and one parallel φ_t . These are given by [2]:

$$\varphi_t = -\frac{1}{n} \frac{dn}{dT} \int_0^{\infty} \delta \sin(\delta y) E(\delta) \exp(-\beta_f z) \exp(i\alpha x) d\delta \hat{k}, \quad (2.13)$$

$$\varphi_n = \frac{1}{n} \frac{dn}{dT} \int_0^{\infty} \beta_f \cos(\delta y) E(\delta) \exp(-\beta_f z) \exp(i\alpha x) d\delta \hat{l}, \quad (2.14)$$

with $dn/dT < 0$.

As there are no known analytical solutions for the integrals (2.12) – (2.14), Salazar et al. [6] have derived a set of linear relations between easily measurable magnitudes, whose slope gives directly the thermal diffusivity. Care should be taken however in using these relations, as some are only valid when the photothermal parameters a , b and z_0 are zero. These relations as applicable to the used mirage setup (figure 2.1) are

$$\psi(T_{ss}) = -\sqrt{\frac{\pi f}{D_s}} y_0, \quad (2.15)$$

the linear relation between the phase of the sample surface temperature $\psi(T_{ss})$ and the pump to probe offset y_0 under the condition $a=b=0$;

$$\psi(\varphi_t) = -\sqrt{\frac{\pi f}{D_s}} y_0, \quad (2.16)$$

the linear relation between the phase of the transverse deflection $\psi(\varphi_t)$ and the pump to probe offset y_0 under the condition $a=b=z_0=0$;

$$\psi(\varphi_n) = -\sqrt{\frac{\pi f}{D_f}} z_0, \quad (2.17)$$

the linear relation between the phase of the normal deflection $\psi(\varphi_n)$ and the probe beam height z_0 under the condition $a=b=y_0=0$;

$$d_{ss} = \sqrt{\frac{\gamma \pi D_s}{f}}, \quad (2.18)$$

the linear relation between the distance d_{ss} between the first noncentral zero crossings of the real part of the surface temperature $Re(T_{ss})$ and the inverse root frequency under the condition $a=b=0$, with $\gamma=1.00$ for opaque thermally thick materials and $\gamma=0.562$ for opaque thermally thin materials and transparent materials. There is no linear relation for intermediate cases;

$$d_t = \sqrt{\frac{\gamma \pi D_s}{f}}, \quad (2.19)$$

the linear relation between the distance d_t between the first noncentral zero crossings of the real part of the transverse deflection $Re(\varphi)$ and the inverse root frequency under the condition $a=b=z_0=0$, with $\gamma=1.44$ for opaque thermally thick materials and $\gamma=1.00$ for opaque thermally thin materials and transparent materials. There is no linear relation for intermediate cases.

In order to classify materials according to thermal thickness and optical transparency the thermal diffusion length $\mu_s=(D_s/\pi f)^{1/2}$ and optical length $\mu_\alpha=l/\alpha$ are introduced. A sample is

- optically opaque when $\mu_\alpha/\mu_s \leq 0.025$;
- optically transparent when $\mu_\alpha/\mu_s \geq 100$;
- thermally thick when $l/\mu_s > 2.5$;
- thermally thin when $l/\mu_s < 0.5$,

with l the sample thickness.

Note that the theoretical model used above is based on a geometrical optics approach.

However for modulation frequencies below $\sim 300\text{Hz}$ the differences between the geometrical and wave optics models are insignificant [7]. As the used frequencies are in the frequency range of 8-25Hz the model can be applied.

3. Experimental setup for Mirage measurements

In this chapter the used setup is described. In 3.1 the general setup and the individual components are examined. The specific operation of the setup for optimization with regard to vibrations is given in 3.2.

3.1. Description of the individual parts

The general setup as used in this work is given schematically in figure 3.1.

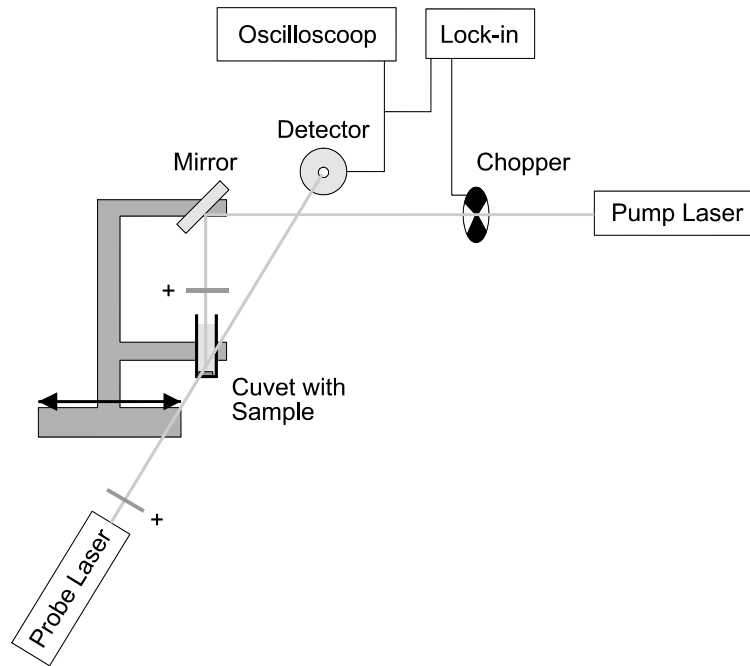


fig. 3.1: used setup for mirage deflection

The following components are used:

- The pump beam is generated by a Liconix argon ion laser, with a wavelength of $\lambda=488\text{nm}$. The laser is operated at 60mW.
- The pump beam is modulated by a HMS 230 light beam chopper, operating in a frequency range of 4Hz-200Hz. The blade jitter is $\pm 0.2^\circ$.
- The sample is contained in a quartz cuvet and immersed in the coupling fluid. The coupling fluid used is CCl_4 , fabricated by Merck. This has the following parameters: $k = 0.099 \text{ Wm}^{-1}\text{K}^{-1}$ at 25°C , $D = 0.731 \cdot 10^{-7} \text{ m}^2\text{s}^{-1}$, $n = 1.460$ and $dn/dT = -6.12 \cdot 10^4 \text{ K}^{-1}$ [14].
- The cuvet is mounted on a translator. This translates pump beam relative to the probe beam in a straight line with an accuracy of $\pm 10\mu\text{m}$.
- The sample is probed by a Spectra Physics He-Ne laser with a wavelength of $\lambda=632.8\text{nm}$. The power is 3mW, which is obtained by a measurement. The power should be 10mW according to the specifications.
- The detector is composed of a plastic fiber with a diameter of $1000\mu\text{m}$. The fiber tip surface is irradiated by the probe beam. As this probe beam gets deflected, the intensity on the fiber tip will change as a result of the Gaussian profile of the probe beam. The light that passes through the filter goes then through a monochromator (McPherson, 0.25m) to filter out the light of a wavelength of $\lambda=632.8\text{nm}$, the wavelength of the probe beam. The signal is then received by an Oriel Photomultiplier Tube, which is powered by a 740V power supply.

- A Stanford Research Systems SR830 DSP Lock-in amplifier is used to compare the phase of the deflection signal with the phase of the reference (chopper). The change in the phase difference is measured as the total phase difference is not only dependent on the position of the probe beam, but also on the phase differences imposed by the used devices and differences in optical path lengths.
- An oscilloscope (LT Gould Digital Storage Oscilloscope, 20MHz) is used for reference and to gain insight in the behavior of the deflection signal.
- Lenses can be used to focus either the pump or probe beam on the sample.
- The setup is made less sensitive to vibrations by placing the table on which the setup is placed on a rubber mat, with its legs placed in a bucket of sand.

3.2. Operation of the setup

In arranging and operating the setup as described in 3.1, two facts have to be taken into account. As the measurements are very sensitive to vibrations the setup should be as stable as possible. Besides this the accuracy and sensitivity of the position measurements should be as good as possible. To this end three different variants of the above setup have been operated.

In the first variant the argon laser is used both for the pump as for the probe beam. A beam splitter is used and the probe beam is attenuated as not to influence the heat distribution due to the pump beam. The usage of the optical instruments and mirrors makes the setup more sensitive to vibrations. Moreover, the fact that both pump and probe beam are of the same color makes it more difficult to align the setup with respect to the crossing point on the sample.

In a second variant the mirror that directs the pump beam moves together with the sample. Again the weight of total setup that has to be moved makes it sensitive to vibrations and less accurate in position.

In a third variant only the mirror that directs the pump beam is moved. This setup is the least sensitive to vibrations as only one light component (the mirror) is moved. Moreover the reading of the position of this light component can be done more accurately as more sensitive devices can be used for moving light components.

In these three variants the setup can be made less sensitive to vibrations by removing the focal lens of the pump and/or probe beam. The negative effects of the finite size of these beams on the measurements, as described in 2.3, are reviewed in 5.3.

The second and third variant have the advantages of a fixed position of the probe beam with respect to the fiber tip of the detector. This is discussed in 6.1.2.

4. Experimental results

To gain insight in the used setup bulk GaAs is used for some preliminary measurements. The results of this measurement are given in 4.1. The particular problems involved with the used setup as well as with the particular sample are given in 4.2. The results of the measurements on a two-layered sample GaAs with a Si-doped GaAs layer are given in 4.3.

4.1. Thermal diffusivity of GaAs and InP

The general procedure to obtain the thermal diffusivity of a sample with the mirage effect is based on (2.16) or (2.19). For these procedures a direction sensitive detector is needed, as the transverse component has to be measured. In this case the used detector does not distinguish between the transverse and normal direction. Moreover the deflection in the normal direction is much larger than the deflection in the transverse direction. As a result the total deflection signal behaves like the normal deflection. Their phases are the same.

To obtain the thermal diffusivity, (2.15) is used and the phase of the total deflection is assumed to be proportional to the phase of the temperature. So

$$\psi(\varphi) = -\sqrt{\frac{\pi f}{D_s}} y_0, \quad (4.1)$$

with φ the total deflection. This assumption is correct as the normal deflection dominates the total deflection and the normal deflection is largest when the temperature gradient that the probe beam encounters is largest. Again it should be the case that $a=b=z_0=0$.

In practice the phase of the deflection is plotted against the position of the probe beam (the offset y_0). The slope of the straight lines on both sides of the center is calculated with Origin 5.0 to obtain the thermal diffusivity with (4.1).

The results of the measurements on GaAs are given in figure 4.1. The setup with scanning pump beam is used as discussed in 3.2.

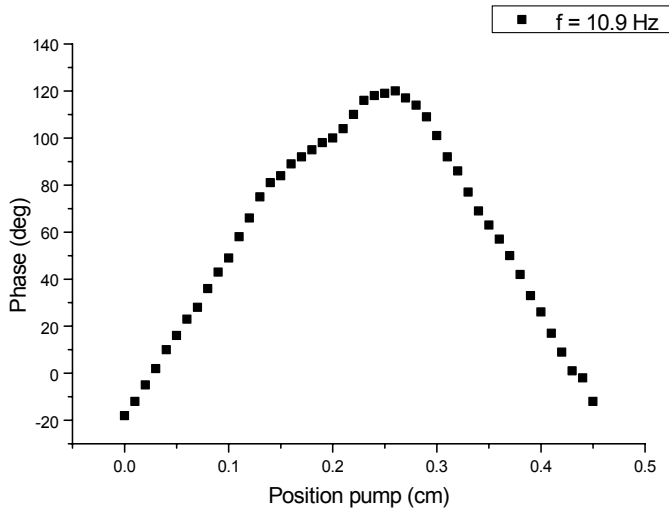


fig 4.1: GaAs with focused pump beam. Scanning pump beam. $f=10.9\pm 0.1\text{Hz}$

Calculation of the thermal diffusivity leads to the following results.

side	points used	slope (Origin 5.0)	thermal diffusivity
left	11	675.45455±6.29107 deg/cm	0.247±0.007 cm ² /s
right	14	-750.32967±9.68115 deg/cm	0.200±0.007 cm ² /s
combined	n.a.	n.a.	0.221±0.007 cm ² /s

The ‘combined’ result combines both slopes and takes the possible tilted state of the sample with respect to the scanning direction into account. This is explained in more detail in 4.2. The results match the value of 0.21-0.26 cm²/s as found in the literature [11].

Also a S-doped InP sample is examined (carrier concentration 4.0-4.7·10¹⁸/cm³). The results are given in figure 4.2.

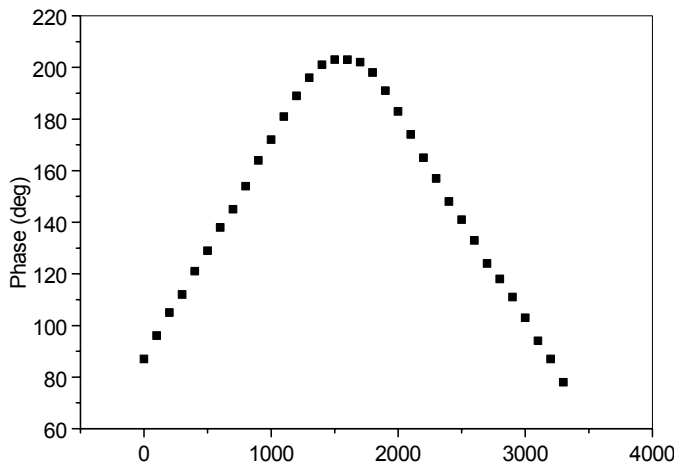


fig. 4.2: InP with focused pump beam. Scanning pump beam. $f=25\text{Hz}$

side	points used	slope (Origin 5.0)	thermal diffusivity
left	12	0.08469±6.07359E-4 deg/μm	0.359±0.006 cm ² /s
right	14	-0.07916±6.97203E-4 deg/μm	0.411±0.006 cm ² /s
combined	n.a.	n.a.	0.384±0.006 cm ² /s

For this specific sample no literature values exist. Pure InP has a thermal diffusivity of 0.46 cm²/s. Apparently the dopant lowers the thermal diffusivity.

4.2. Specific experimental problems concerning the Mirage effect

The used Mirage setup has some specific shortcomings which will be discussed in here. In 4.2.1 the effect of the tilted position of the sample as compared to the scanning direction will be discussed. In 4.2.2 the effect on the Mirage signal of irregularities on the sample surface will be discussed. Finally another method of determining the thermal diffusivity using the same setup is reviewed. This method aims to get more accurate results and is discussed in 4.2.3.

4.2.1. Tilted sample

Preliminary measurements with the GaAs sample using the setup in which the pump beam and the sample move together (i.e. the probe beam stays in position) gave the results as depicted in figure 4.3.

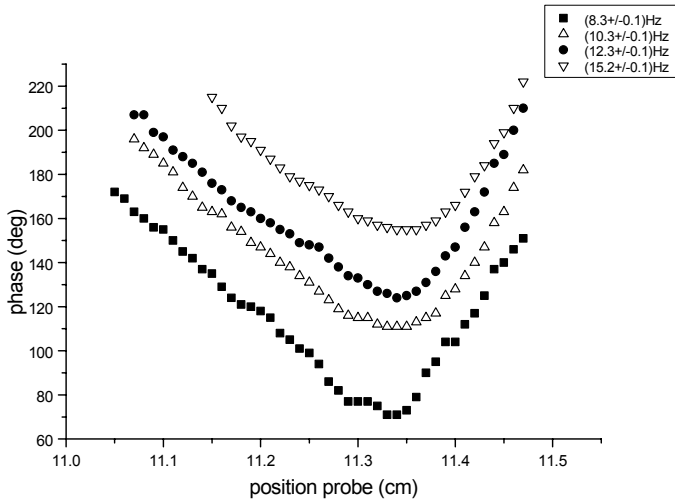


fig. 4.3: Phase of deflection vs. position probe beam. The sample under study is GaAs.

Although the results are rather inaccurate compared to the results in figures 4.1 and 4.2, the difference in slopes in the parts of the graphs left and right of the center is evident.

Theoretically the slopes should be the same as the sample is isotropic to the travelling thermal wave. The difference in the slopes is assumed to be due to the fact that the sample is in a tilted position with regard to the plane of scanning. This leads to a gradual change in the vertical offset z_0 when scanning over the sample surface which imposes an additional, gradually changing phase difference.

As this vertical offset z_0 changes linearly with position of the scanning probe beam and as the thermal wave travels faster in the sample medium than in the coupling medium, the thermal diffusivity can be calculated by taking the average of both slopes, not by taking the average of the thermal diffusivities as calculated for both individual slopes.

Notwithstanding this theory the sample should be placed as parallel as possible to the plane of scanning as an increase in vertical offset z_0 heavily weakens the signal. Less measurement points can be taken as can be seen on the right side slopes in figure 4.3.

This method of averaging the slopes is used in calculating the thermal diffusivities in 4.1.

4.2.2. Irregularities on the sample surface

The figures 4.4 and 4.5 show the results of measurements in which the pump beam scans the sample surface. Both measurements are taken directly after each other and only the frequency is changed (25Hz and 15Hz respectively).

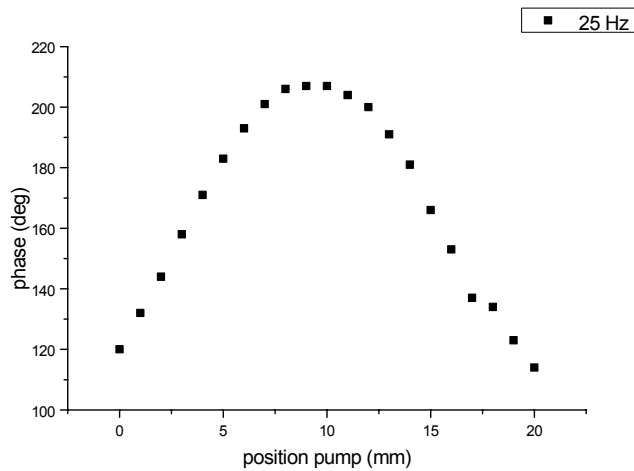


fig. 4.4: Phase of deflection vs. position pump beam. The sample under study is GaAs. The modulation frequency used is 25 Hz.

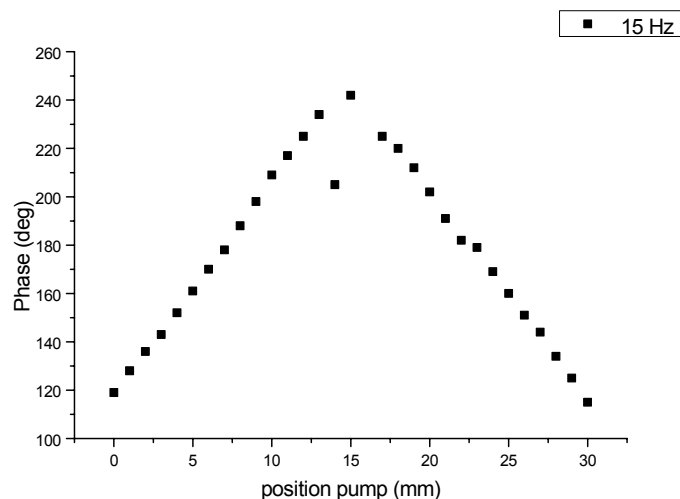


fig. 4.5: Phase of deflection vs. position pump beam. The sample under study is GaAs. The modulation frequency used is 15 Hz.

Both graphs have a discontinuity in the right hand side, at the same position of the center. This is assumed to be due to the fact that the surface has a scratch on this position. Careful review of the sample surface shows that this is indeed the case.

4.2.3. Other method for determining the thermal diffusivity

Finally another method of determining the thermal diffusivity using the same setup is reviewed. This method aims to get more accurate results and is discussed in 4.2.3.

The used setup is very difficult to align: the strength of the signal is heavily dependent on the position of the detector with regard to the probe beam and a slightly tilted position of the sample restricts the number of measurement points on one side as discussed in 4.2.2. As the method of determining the thermal diffusivity is only dependent on the linearity as follows from (4.1), the measurement of only two or three very accurate points will suffice.

To get those very accurate points $\psi(\varphi)$ is plotted against $f^{1/2}$ with the other parameters kept constant in (4.1). As the exact position y_0 is not known, two or three series of measurements have to be taken. The results are shown in figure 4.6. Care should be taken that the chosen points are well outside the center area and in the region where the linearity holds.

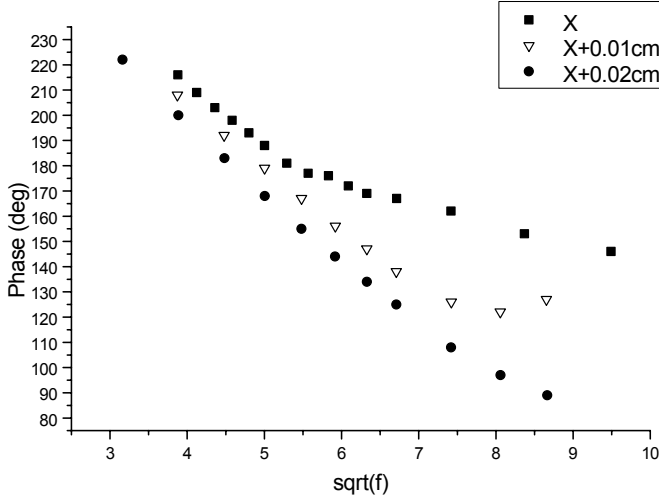


fig. 4.6: Phase of deflection vs. modulation frequency pump beam . The sample under study is GaAs. Measurements are taken at three positions outside the heating spot, each $100\mu\text{m}$ apart.

The measurements do not show the linearity as can be expected from (4.1). This is due to the fact that theoretically (4.1) only holds when the vertical offset z_0 equals zero. There are two options for reducing the impact of a finite z_0 . The first option is to scan the surface with the probe beam as close as possible to the surface. The second option is to increase the thermal diffusion length $\mu_s = (D_s/\pi f)^{1/2}$ (according to 2.3), which also lowers the effects of a nonzero z_0 offset.

Figure 4.6 shows the effect of a varying thermal diffusion length. To gain the correct value of the thermal diffusivity, the limiting slope for low values of the frequency f should be taken in the graph through the measurement points in figure 4.6 instead of the slope of a linear graph through all measurement points [11]. Taking a limiting slope does not give accurate results as compared to the results generated in 4.1. As a conclusion this method is not used.

4.3. Experimental results with 2-layered samples

The same setup as used in 4.1 is used to gain the Mirage signal of a sample that is composed of two epitaxial layers. The sample studied is composed of a $400\mu\text{m}$ semi-insulating GaAs substrate with a $6\mu\text{m}$ epitaxial layer of Si-doped GaAs (carrier concentration $n=5 \cdot 10^{14}/\text{cm}^3$). The results of the sample with the doped layer on top are given in the figures 4.7 and 4.8.

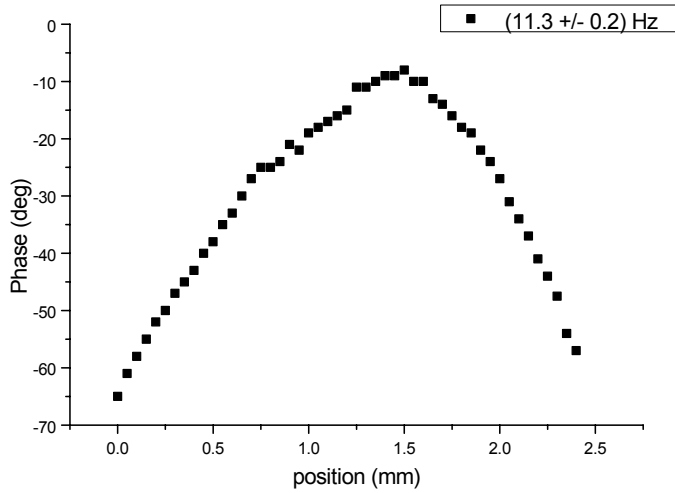


fig. 4.7: Phase of deflection vs. position pump beam. The sample under study is SI GaAs ($400\mu\text{m}$) with a Si doped GaAs layer of $6\mu\text{m}$.

side	points used	slope (Origin 5.0)	thermal diffusivity
left	13	51.64835 ± 1.09088 deg/mm	0.44 ± 0.03 cm^2/s
right	10	-73.0303 ± 2.20276 deg/mm	0.22 ± 0.02 cm^2/s
combined	n.a.	n.a.	0.30 ± 0.03 cm^2/s

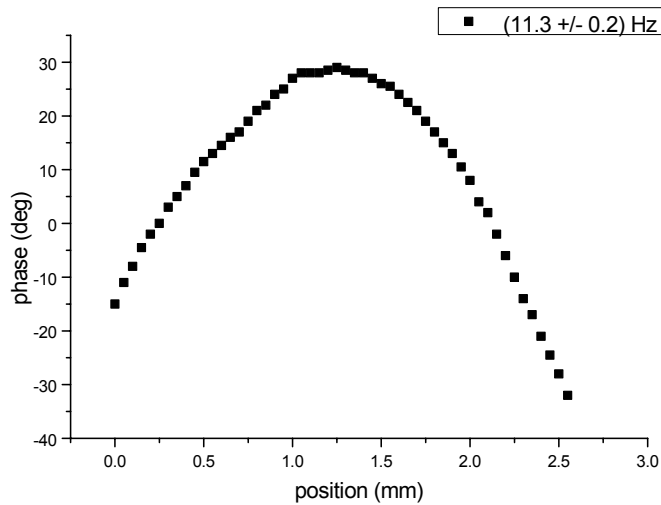


fig. 4.8: Phase of deflection vs. position pump beam. The sample under study is SI GaAs ($400\mu\text{m}$) with a Si doped GaAs layer of $6\mu\text{m}$. Sample rotated clockwise over 180° as compared to fig. 4.7.

side	points used	slope (Origin 5.0)	thermal diffusivity
left	4	69 ± 2.64575 deg/mm	0.24 ± 0.03 cm^2/s
right	10	-74.72727 ± 0.73481 deg/mm	0.21 ± 0.02 cm^2/s
combined	n.a.	n.a.	0.23 ± 0.03 cm^2/s

The graphs in figures 4.7 and 4.8 seem to be more curved than the graphs in figures 4.1 and 4.2. This fact has two consequences. First the measurement of the slope becomes less accurate due to the fact that the points are not or only in the regions far from the center arranged in a straight line. Secondly the question arises whether the thermal diffusivity can be calculated

from the slope of the graphs, i.e. whether the relationship between the position and the phase as given in (4.1) is a linear one.

Also the backside of the sample is illuminated. The results are given in figure 4.9.

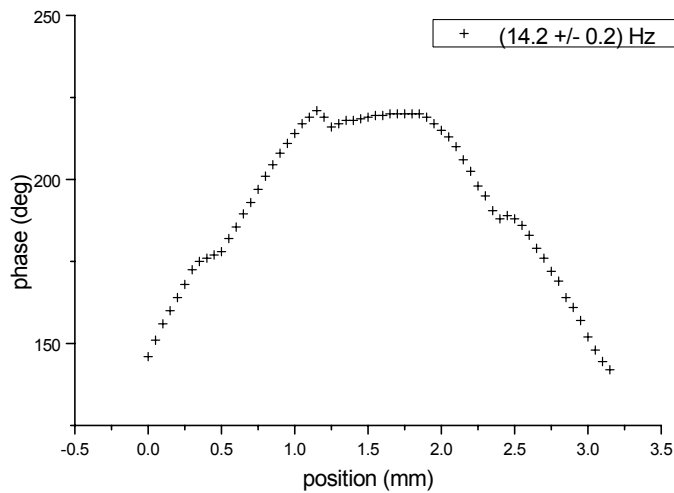


fig. 4.9: Phase of deflection vs. position pump beam. The sample under study is SI GaAs ($400\mu\text{m}$) with a Si doped GaAs layer of $6\mu\text{m}$. Sample turned upside down as compared to fig. 4.7; the substrate layer is illuminated

side	points used	slope (Origin 5.0)	thermal diffusivity
left	6	87.42857 ± 2.4908 deg/mm	0.19 ± 0.02 cm^2/s
right	12	-76.67832 ± 1.09476 deg/mm	0.25 ± 0.01 cm^2/s
combined	n.a.	n.a.	0.22 ± 0.02 cm^2/s

The line of the graph in figure 4.9 is not smoothly curved but shows some ‘bumps’. A possible explanation for this effect is the doping in the sample. Due to the doping (Si in this case) the isotropy of the sample can be disturbed and local irregularities in the thermal diffusivity can arise. The thermal wave has a different speed in these local irregularities. The ‘bumps’ in the graph can be a result of this effect.

Another explanation for the 'bumps' is the result of very low frequency disturbances in the setup. Only the effect of convection in the coupling fluid is a possible explanation for such low frequencies.

For a full understanding of the effects in 2-layered samples and the result of the different parameters, a theoretical model has been developed. This is explained in chapter 5.

5. Theoretical model

To gain understanding in the effects that occur in the Mirage signal of a two-layered sample a theoretical model is developed in this chapter. In 5.1 the equations that govern the heat diffusion in the sample and the surrounding coupling fluids are discussed. A theoretical model for the heat diffusion in multilayered samples in the photoacoustic effect has already been developed [12]. This theory results in equations that can be solved analytically. Contrary to the photoacoustic effect, which is essentially two-dimensional, the Mirage effect is essentially three-dimensional. As a result the theory developed in [12] can not be used. Moreover the set of equations that is derived in 5.1 can not be solved analytically. A Matlab-program is used to solve the equations from 5.1 numerically. The basics of this program are given in 5.2. In 5.3 the program is evaluated on correctness and accuracy. The results of the program are compared with the known behavior of the Mirage deflection in a bulk sample. Finally the theoretical behavior of the Mirage signal of two-layered samples is reviewed in 5.4.

5.1. Theory for a two-layered sample

Analogue to the theory described in Chapter 2 (equations (2.6)-(2.8)) the equations that govern the temperature distribution in a two-layered sample are given by

$$\nabla^2 T_i - \frac{1}{D_i} \frac{\partial T_i}{\partial t} = -\frac{Q_i(r,t)}{k_i}, \quad (5.1)$$

with $i=f, 1, 2, b$ for f : coupling fluid, 1, 2: layer number and b : backing. The heat deposited per unit volume and per unit time in the i th layer, $Q_i(r,t)$, is given by

$$\begin{aligned} Q_1(r,t) &= \frac{2\alpha_1 P_0}{\pi a^2} e^{\alpha_1 z} e^{-2(r/a)^2} e^{j\omega t}, \\ Q_2(r,t) &= \frac{2\alpha_2 P_0}{\pi a^2} e^{\alpha_2 z - l_1(\alpha_1 - \alpha_2)} e^{-2(r/a)^2} e^{j\omega t}, \\ Q_f, Q_b &= 0, \end{aligned} \quad (5.2)$$

with P_0 the input power and l_1 the thickness of layer 1. The assumption is made that the (coupling) fluid and the backing are nonabsorbent to the modulated source ($\alpha_f, \alpha_b = 0$). Note that the geometry of figure 2.2 is used, i.e. z is negative inside the sample and z equals zero on the illuminated sample surface.

Again the boundary conditions are, analogue to Chapter 2

$$\begin{aligned} T_i &= T_j, \\ k_i \frac{\partial T_i}{\partial z} &= k_j \frac{\partial T_j}{\partial z}, \end{aligned} \quad (5.3)$$

on the i - j interface.

To find the analytical expression for the temperature field in the cylindrical geometry, integral transformations such as a 3D Fourier transform [8] or a combination of Hankel and Laplace transformations [1] can be used. The treatment as suggested in [1] is expanded and used in the calculation of the temperature distribution in a two-layered sample.

By replacing the modulated heat source (5.2) by a unit heat source,

$$\begin{aligned}
Q'_1(r, t) &= \frac{2\alpha_1 P_0}{\pi a^2} e^{\alpha_1 z} e^{-2(r/a)^2} \delta(t) = Q'_1(r) e^{\alpha_1 z} \delta(t) \\
Q'_2(r, t) &= \frac{2\alpha_2 P_0}{\pi a^2} e^{\alpha_2 z - \ell_1(\alpha_1 - \alpha_2)} e^{-2(r/a)^2} \delta(t) = Q'_2(r) e^{\alpha_2 z} \delta(t),
\end{aligned} \tag{5.4}$$

is obtained. The factor $e^{\alpha_2 z - \ell_1(\alpha_1 - \alpha_2)}$ in Q'_2 replaces the analogue factor $e^{\alpha_1 z}$ in Q'_1 to account for the fact that energy of the pump beam is dissipated in layer 1.

Next the Hankel transformation

$$\begin{aligned}
T_i(r, z, t) &= T_{0,i}(\delta, z, t) \\
T_{0,i}(\delta) &= \int_0^\infty T_i(r) J_0(\delta r) r dr
\end{aligned} \tag{5.5}$$

is applied to (5.1) in order to reduce the partial differential equations to simpler partial differential equations

$$\begin{aligned}
-\delta^2 T_{0,i}(\delta, z, t) + \frac{\partial^2 T_{0,i}(\delta, z, t)}{\partial z^2} - \frac{1}{D_i} \frac{\partial T_{0,i}(\delta, z, t)}{\partial t} \\
= -Q'_{0,i}(\delta) \exp(\alpha_i z) \delta(t).
\end{aligned} \tag{5.6}$$

where $Q'_{0,i}(\delta)$ is the Hankel transformation of $Q'_i(r)$. The Laplace transformation,

$$T_{0,i}(\delta, z, t) = \mathfrak{S}_{0,i}(\delta, z, p), \tag{5.7}$$

is used to transform the partial differential equations to ordinary differential equations:

$$\begin{aligned}
-\delta^2 \mathfrak{S}_{0,i}(\delta, z, p) + \frac{\partial^2 \mathfrak{S}_{0,i}(\delta, z, p)}{\partial z^2} - \frac{p}{D_i} \mathfrak{S}_{0,i}(\delta, z, p) \\
= -Q'_{0,i}(\delta) \exp(\alpha_i z).
\end{aligned} \tag{5.8}$$

This set of ordinary differential equations in z can be solved. The solutions are:

$$\begin{aligned}
\mathfrak{S}_{0,i}(\delta, z, p) &= A_i(\delta, p) \exp(-\beta_i z) + B_i(\delta, p) \exp(\beta_i z) \\
&\quad + \frac{Q'_{0,i}(\delta) \exp(\alpha_i z)}{\beta_i^2 - \alpha_i^2},
\end{aligned} \tag{5.9}$$

where $\beta_i^2 = \delta^2 + (i\omega/D_i)$. Using the Hankel inversion,

$$T_i(r) = \int_0^\infty T_{0,i}(\delta) J_0(\delta r) \delta d\delta, \tag{5.10}$$

(5.9) is transformed into

$$\begin{aligned} \mathfrak{S}_{0,i}(r, z, p) = & \int_0^{\infty} [A'_i(\delta, p) \exp(-\beta_i z) + B'_i(\delta, p) \exp(\beta_i z) \\ & + \frac{Q'_{0,i}(\delta) \exp(\alpha_i z)}{\beta_i^2 - \alpha_i^2}] J_0(\delta r) \delta d\delta. \end{aligned} \quad (5.11)$$

To find the periodic steady state,

$$T_i(r, z, t) = \mathfrak{S}_{0,i}(r, z, p) \Big|_{p=j\omega} \exp(j\omega t) \quad (5.12)$$

is used to obtain the expressions of the modulated temperature field:

$$\begin{aligned} T_i(r, z, t) = & \int_0^{\infty} [A_i(\delta) \exp(-\beta_i z) + B_i(\delta) \exp(\beta_i z) \\ & + \frac{Q'_{0,i}(\delta)}{\beta_i^2 - \alpha_i^2} \exp(\alpha_i z)] \exp(j\omega t) J_0(\delta r) \delta d\delta, \end{aligned} \quad (5.13)$$

with

$$\begin{aligned} Q'_{0,1} &= \frac{\alpha_1 P_0 \exp\left(-\frac{(\alpha_1 \delta)^2}{8}\right)}{k_1}, \\ Q'_{0,2} &= \frac{\alpha_2 P_0 \exp\left(-\frac{(\alpha_2 \delta)^2}{8}\right)}{k_2} \exp(-\ell_1(\alpha_1 - \alpha_2)), \\ Q'_{0,f}, Q'_{0,b} &= 0. \end{aligned} \quad (5.14)$$

By applying the boundary conditions (5.3) to the four equations ($i=f, 1, 2, b$) and making the assumption that the dimensions of the (coupling) fluid and the backing extend to infinity in respectively the positive and negative z -direction ($B_f, A_b=0$), six equations for the six constants (A_f, A_1, B_1, A_2, B_2 and B_b) are obtained which can be expressed in the following matrix equation (5.15):

$$\begin{pmatrix} 1 & -1 & -1 & 0 & 0 & 0 \\ -k_f\beta_f & k_1\beta_1 & -k_1\beta_1 & 0 & 0 & 0 \\ 0 & e^{\beta_1\ell_1} & e^{-\beta_1\ell_1} & -e^{\beta_2\ell_1} & -e^{-\beta_2\ell_1} & 0 \\ 0 & -k_1\beta_1e^{\beta_1\ell_1} & k_1\beta_1e^{-\beta_1\ell_1} & k_2\beta_2e^{\beta_2\ell_1} & -k_2\beta_2e^{-\beta_2\ell_1} & 0 \\ 0 & 0 & 0 & e^{\beta_2\ell_2} & e^{-\beta_2\ell_2} & -e^{-\beta_3\ell_2} \\ 0 & 0 & 0 & -k_2\beta_2e^{\beta_2\ell_2} & k_2\beta_2e^{-\beta_2\ell_2} & -k_3\beta_3e^{-\beta_3\ell_2} \end{pmatrix} \times \begin{pmatrix} A_f \\ A_1 \\ B_1 \\ A_2 \\ B_2 \\ B_b \end{pmatrix} = \begin{pmatrix} \frac{Q'_{0,1}(\delta)}{\beta_1^2 - \alpha_1^2} \\ k_1\alpha_1 \frac{Q'_{0,1}(\delta)}{\beta_1^2 - \alpha_1^2} \\ \frac{Q'_{0,2}(\delta)e^{-\alpha_2\ell_1}}{\beta_2^2 - \alpha_2^2} - \frac{Q'_{0,1}(\delta)e^{-\alpha_1\ell_1}}{\beta_1^2 - \alpha_1^2} \\ k_2\alpha_2 \frac{Q'_{0,2}(\delta)e^{-\alpha_2\ell_1}}{\beta_2^2 - \alpha_2^2} - k_1\alpha_1 \frac{Q'_{0,1}(\delta)e^{-\alpha_1\ell_1}}{\beta_1^2 - \alpha_1^2} \\ - \frac{Q'_{0,2}(\delta)e^{-\alpha_2(\ell_1+\ell_2)}}{\beta_2^2 - \alpha_2^2} \\ k_2\alpha_2 \frac{Q'_{0,2}(\delta)e^{-\alpha_2(\ell_1+\ell_2)}}{\beta_2^2 - \alpha_2^2} \end{pmatrix} \quad (5.15)$$

With this matrix equation the coefficient A_f can be calculated. This leads to the following expressions for the temperature field and the normal and transverse deflection [3], [8]:

$$T_f(y, z, t) = \frac{1}{2\pi} \int_0^{\infty} J_0(\delta y) A_f(\delta) \exp(-\beta_f z) \delta d\delta \exp(i\omega t), \quad (5.16)$$

$$\varphi_n = -\frac{1}{\pi n} \frac{dn}{dT} \int_0^{\infty} \cos(\delta y) A_f(\delta) \exp(-\beta_f z) \beta_f d\delta \exp(i\omega t), \quad (5.17)$$

$$\varphi_t = -\frac{1}{\pi n} \frac{dn}{dT} \int_0^{\infty} \sin(\delta y) A_f(\delta) \exp(-\beta_f z) \delta d\delta \exp(i\omega t), \quad (5.18)$$

5.2. Model

As the equations (5.16)-(5.18) cannot be solved analytically a computer is used for a numerical calculation. A calculation as suggested in [9], based on a series expansion [10], cannot be used. The matrix inversion used to obtain A_f out of (5.15) gives singularities when used in the series expansion. This is a result of the exponential dependency of A_f on δ . This limits the amount of terms that can be used severely to below the required number to gain the necessary accuracy [9].

The following approach is chosen. At first the matrix equation (5.15) is solved analytically to obtain A_f . Hereafter the equation is rearranged to prevent the occurrence of singularities with the variation of δ . At last a program is written in Matlab to calculate (5.16)-(5.18) numerically and to evaluate the results.

By solving the matrix equation (5.15) the coefficient A_f can be expressed in the following way:

$$A_f = -\frac{\langle 2 \rangle - \langle 3 \rangle \cdot \langle 1 \rangle}{1 + k_f \beta_f \cdot \langle 1 \rangle}, \quad (5.19)$$

in which

$$\langle 1 \rangle = \frac{1}{k_1 \beta_1} \left(\frac{1 - e^{2\beta_1 \ell_1} \left(\frac{1 - c_2 \Gamma}{1 + c_2 \Gamma} \right)}{1 + e^{2\beta_1 \ell_1} \left(\frac{1 - c_2 \Gamma}{1 + c_2 \Gamma} \right)} \right), \quad (5.20)$$

$$\langle 2 \rangle = -\frac{Q'_{0,1}(\delta)}{\beta_1^2 - \alpha_1^2} + \left(\frac{\Lambda}{e^{-\beta_1 \ell_1} (1 + c_2 \Gamma)} \right), \quad (5.21)$$

$$\langle 3 \rangle = -k_1 \alpha_1 \frac{Q'_{0,1}(\delta)}{\beta_1^2 - \alpha_1^2} + k_1 \beta_1 \left(\frac{\Lambda}{e^{-\beta_1 \ell_1} (1 + c_2 \Gamma)} \right), \quad (5.22)$$

$$\Gamma = \frac{1 + e^{2\beta_2(\ell_2 - \ell_1)} \left(\frac{1 + c_3}{1 - c_3} \right)}{1 - e^{2\beta_2(\ell_2 - \ell_1)} \left(\frac{1 + c_3}{1 - c_3} \right)}, \quad (5.23)$$

$$\Lambda = \frac{Q'_{0,1}(\delta) e^{-\alpha_1 \ell_1}}{\beta_1^2 - \alpha_1^2} \left(1 + \frac{k_1 \alpha_1}{k_2 \beta_2} \Gamma \right) - \frac{Q'_{0,2}(\delta) e^{-\alpha_2 \ell_1}}{\beta_2^2 - \alpha_2^2} \left(1 + \frac{k_2 \alpha_2}{k_2 \beta_2} \Gamma \right) + \frac{Q'_{0,2}(\delta) e^{-\alpha_2(\ell_1 + \ell_2)}}{\beta_2^2 - \alpha_2^2} e^{-\beta_2 \ell_1} \left(\frac{1 - \frac{k_2 \alpha_2}{k_3 \beta_3}}{1 - c_3} \right) (1 + \Gamma), \quad (5.24)$$

with

$$c_1 = \frac{k_0 \beta_0}{k_1 \beta_1}; \quad c_2 = \frac{k_1 \beta_1}{k_2 \beta_2}; \quad c_3 = \frac{k_2 \beta_2}{k_3 \beta_3}. \quad (5.25)$$

Equations (5.19)-(5.25) are used in the Matlab program (see Appendix B).

5.3. Evaluation of the Model

In general the model has to comply with two demands: it should be correct, both physically and analytically, and it should be accurate. These demands are reviewed in the next paragraphs.

5.3.1. Accuracy of the model

For testing the accuracy a graph (figure 5.1) is made with the program and evaluated. Two regions are to be examined, namely the region outside the two oscillating regions and the two oscillating regions itself.

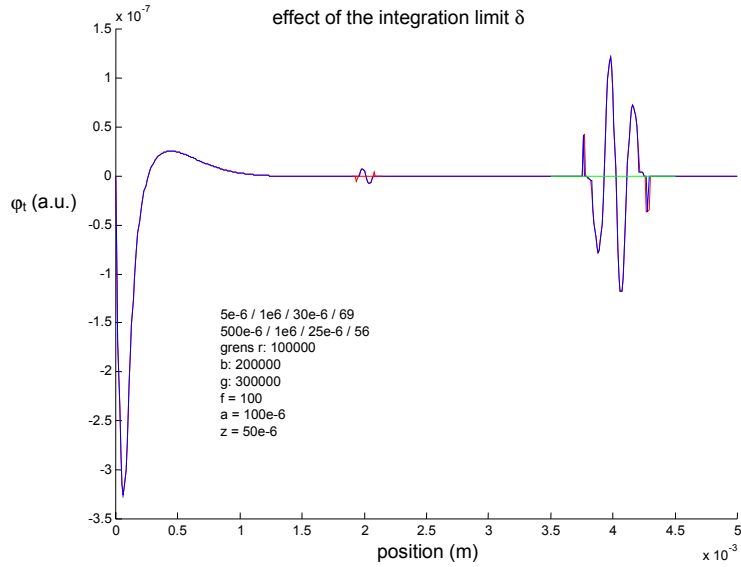


fig. 5.1: effect of integration limit δ

Considering the region outside the two oscillating regions in figure 5.1, insight is gained in the accuracy of the computer model. Comparing the graphs of the function (5.18) with integral limits of zero to respectively $\delta=100000$ and $\delta=200000$ and measuring the difference between the graphs errors are obtained of $<10^{-11}$ for the top of the first minimum, $<3 \cdot 10^{-12}$ for the top of the first maximum and $<10^{-14}$ for the horizontal part. This leads to relative errors of less than 0.5% for the graph using $\delta=100000$. The difference between the graphs of the function (5.18) with integral limits of zero to respectively $\delta=200000$ and $\delta=300000$ is less than 0.01%. This calculation is important as δ has a big influence on the calculation time with the Matlab program, so δ should be as small as possible within certain limits for the accuracy.

The two oscillating regions at $\delta=100000$ are unexpected. They are removed from the graph when the integration limit is raised to $\delta=300000$, as can be seen in figure 5.2. This means that they do not occur as a result of singularities in the model.

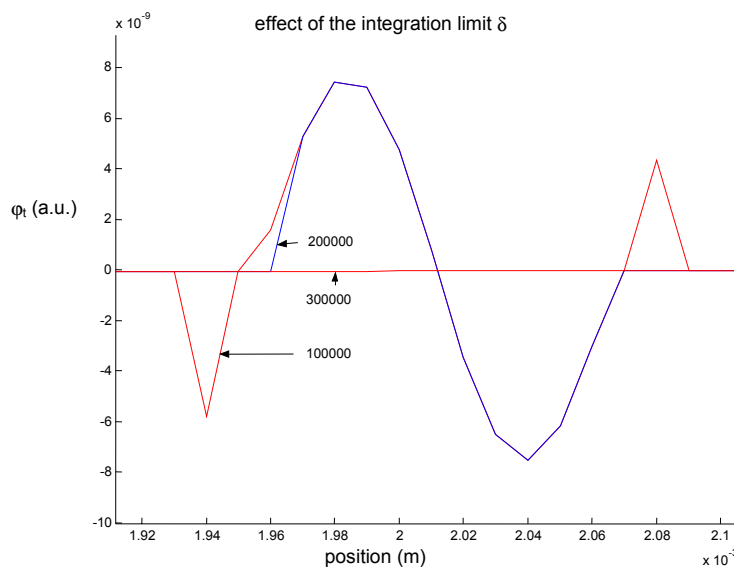


fig. 5.2: effect of integration limit δ in the oscillating region. Values for δ are taken at 100000, 200000, 300000.

Generally $\delta=100000$ or $\delta=200000$ is considered to be accurate enough, unless unexpected oscillations as in figure 5.1 occur. The occurrence of these oscillations cannot be predicted as they depend on different parameters. Such oscillations (or deviations from the expected graph) need to be analyzed with $\delta=300000$.

5.3.2. Analytical correctness of the model

As for the analytical correctness there are two possible ways of testing. The model should not be dependent on the position of the separation between two layers when both are given the same values for the physical parameters. In effect the sample becomes a bulk sample. This is the case both mathematically as the parameter l_1 disappears from the equation (5.19) as well as in the computer model, which plots the same graphs for different values of l_1 . Additionally this is a test for the correctness of the used syntax and structure in the program.

It should be noted that this test is not sufficient proof for the validity of the model. On the other hand, when this test is not passed, the derived equation (5.19) or the syntax of the program or both are incorrect. As such the test is useful for debugging.

5.3.3. Physical correctness of the model

For testing the physical correctness of the model the results obtained with the program (plotted graphs) can be compared to the already known behavior of the Mirage deflection in samples with a known thermal diffusivity. Unfortunately there is no literature concerning the mirage deflection of multilayer samples. As a result these data can not be tested. Additionally the results (plots) can be used to gain insight in the effect of the practical concessions that have to be made towards the theoretical condition $a=b=z_0=0$ for applying (4.1).

First a plot is made of the temperature versus the off-center position (figure 5.3).

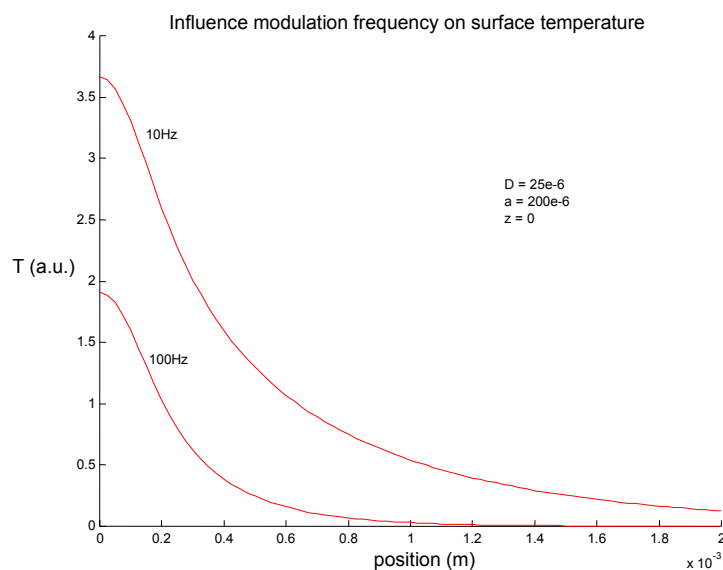


fig. 5.3: plot of the absolute temperature vs. the off-center position at two different modulation frequencies

The shape is according to the expectations with a large temperature amplitude in the center and decreasing amplitude towards the edges of the sample. In this case the absolute value of the temperature is plotted. Unfortunately the shape of the curve is a very qualitative aspect. To get quantitative information (and to do a quantitative test), a plot is made of the phase of the transverse deflection versus the off-center position (figure 5.4).

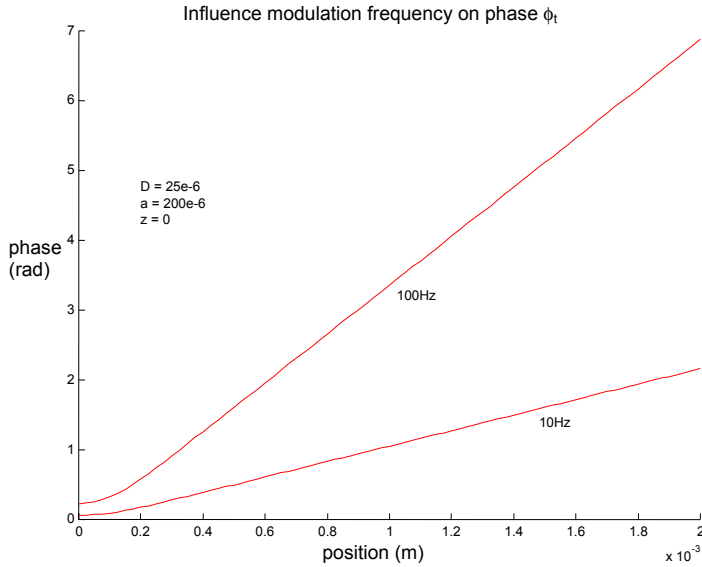


fig. 5.4: plot of the phase of the transverse deflection vs. the off-center position at two different modulation frequencies

According to the theory (equation (2.16)), the slope of the plot should give the thermal diffusivity of the sample. A calculation gives the input thermal diffusivity of $D=0.25\text{cm}^2/\text{s}$, which gives additional proof for the correctness of the model and program.

As stated above, in addition to testing the model the results (plots) can be used to gain insight in the effect of the practical concessions that have to be made towards the theoretical condition $a=b=z_0=0$ for applying (4.1). First the effect of the size of the pump beam is reviewed (figure 5.5).

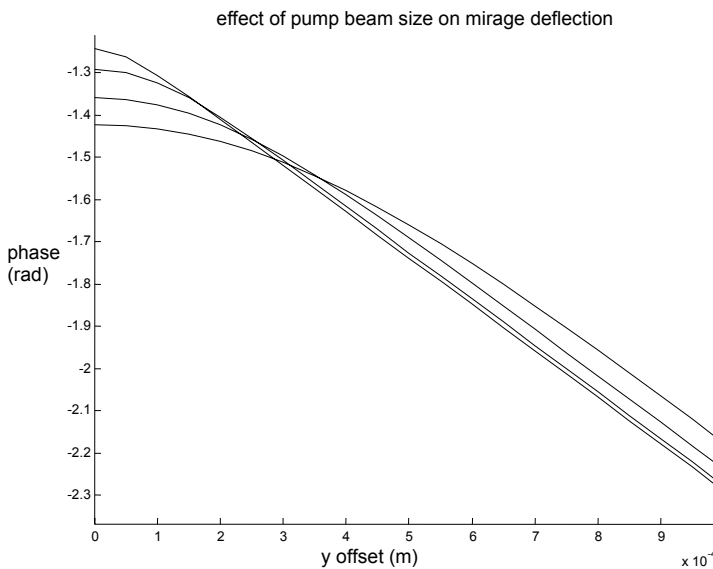


fig. 5.5: influence of pump beam size on the phase of the normal deflection for $a = 0, 200, 400$ and $600\mu\text{m}$.

It can be seen that even for a relatively large diameter of the pump beam ($600\mu\text{m}$) there is a linearity between the phase and the off-center position. So (2.16) holds even for a unequal to zero. On the other hand the range of linearity starts further away from the center. So less measurement points can be taken when a increases (measurements become less accurate when taken further away from the center).

Secondly the effect of nonzero z_0 is reviewed (figure 5.6).

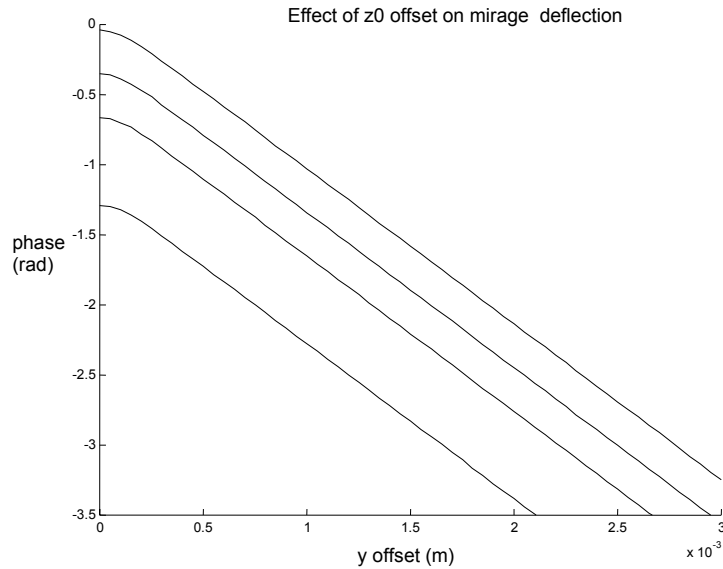


fig. 5.6: influence of z_0 offset on the phase of the normal deflection for $z_0 = 0, 25, 50$ and $100\mu\text{m}$.

As can be expected the absolute phase changes as a result of the extra distance the thermal wave has to travel. The phase difference when going off-center is the same and as a result the slope is the same. So z_0 can be nonzero with (2.16) still holding.

As the probe beam diameter b is not part of the model, its influence can not be reviewed in this way.

Concluding it can be assumed that the model is correct. Also the finite value of z_0 and a is reviewed and assumed to be of no influence on (2.16) and (4.1) when using the setup as explained above (chapter 3).

5.4. Two layers: interpretations

The model as reviewed in 5.3 is used to gain insight in the behavior of the Mirage signal in a two-layered sample. These theoretical results are necessary to fully understand the experimental results obtained in 4.3. This is reviewed in chapter 6.

The calculated phase of the transverse Mirage deflection of a sample with a $400\mu\text{m}$ substrate ($D=0.25\text{cm}^2/\text{s}$) and a $6\mu\text{m}$ top layer with a varying thermal diffusivity is given in figure 5.9.

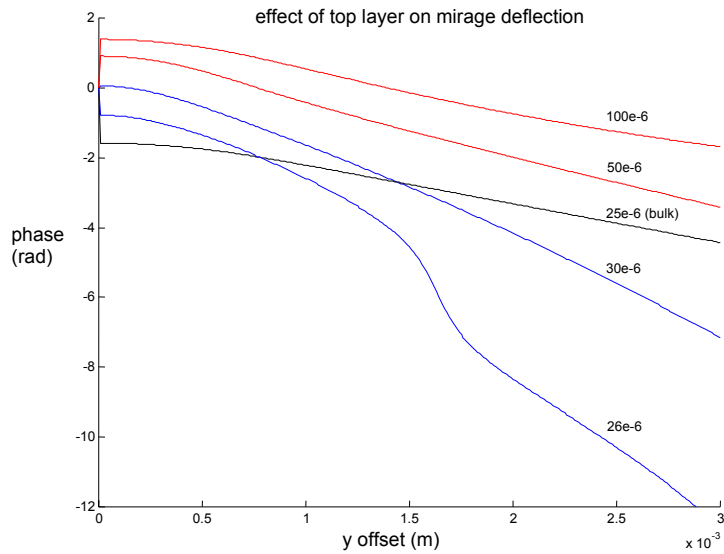


fig. 5.7: influence of the thermal diffusivity of the top epitaxial layer ($6\mu\text{m}$) on a substrate layer ($400\mu\text{m}$, $D=0.25\text{cm}^2/\text{s}$) on the phase of the transverse deflection. $a=600\mu\text{m}$, $z=100\mu\text{m}$, $f=10\text{Hz}$.

The differences in the deflection signal as a result of varying the thermal diffusivity of the top layer are clearly visible. Also there seem to be no regions of linearity which makes the determination of the thermal diffusivity of a two-layered sample in practice very hard. Only when the thermal diffusivity of the substrate layer is known the thermal diffusivity of the top layer can be found by comparing the practically resulting plot with the theoretical plot. Also the Mirage deflection is calculated with the sample turned upside down, i.e. with the pump beam illuminating the substrate. The results are given in figure 5.8.

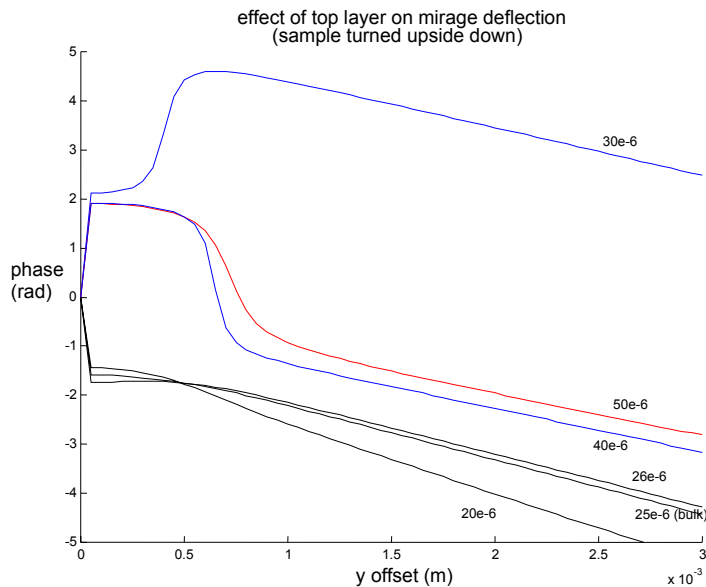


fig. 5.8: influence of the thermal diffusivity of the top epitaxial layer ($6\mu\text{m}$) on a substrate layer ($400\mu\text{m}$, $D=0.25\text{cm}^2/\text{s}$) on the phase of the transverse deflection. $a=600\mu\text{m}$, $z=100\mu\text{m}$, $f=10\text{Hz}$. The sample is turned upside down as compared to fig. 5.7.

Given the fact that the thickness of the substrate layer is far greater than the thickness of the top layer, a similar result as with a pure sample can be expected. This is not the case as can be seen. Clearly the thin top layer (although placed at the backside) plays a big role in the resulting Mirage deflection.

On the other hand clear regions of linearity can be discerned in which the slope is the same over a broad range of top layer thermal diffusivities. Calculation of the slopes with 30E-6, 40E-6 and 50E-6 (see figure 5.8) gives an effective thermal diffusivity of $D = 36 \cdot 10^{-6} \text{m}^2/\text{s}$. Concluding it can be said that only when the thermal diffusivity of the top layer is larger ($\geq 0.05 \text{cm}^2/\text{s}$) than the thermal diffusivity of the substrate layer, relevant information can be obtained from a sample with no known thermal diffusivities.

Besides the general behavior of the deflection signal as explained above, the model can be used to have an in depth look at the phenomenon that occurs at the plot of 26E-6 in figure 5.7. The general shape seems to differ from the plots with other diffusivities. To look at this effect more closely a plot is made of the effect of thermal diffusivities of the top layer close to the one of the substrate layer. The temperature distribution is reviewed. The results are given in figure 5.9.

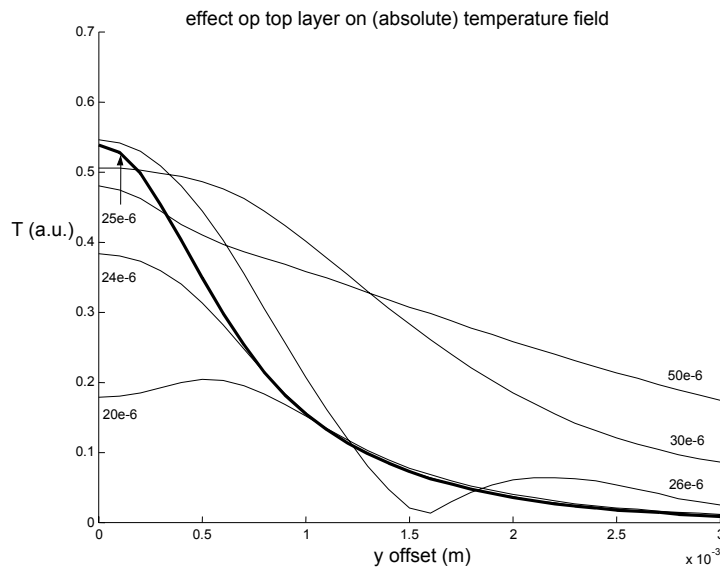


fig. 5.9: influence of the thermal diffusivity of the top epitaxial layer ($6 \mu\text{m}$) on a substrate layer ($400 \mu\text{m}$, $D=0.25 \text{cm}^2/\text{s}$) on the absolute temperature field. $a=600 \mu\text{m}$, $z=100 \mu\text{m}$, $f=10 \text{Hz}$.

As can be seen the amplitude of the temperature does not decrease from the center to the edges in all cases. Apparently some kind of interference between the heat waves in both layers occurs.

A simple calculation of the thermal diffusion length $\mu_s = (D_s/\pi f)^{1/2}$ (according to 2.3) gives for the thermal diffusivities of $0.25 \text{cm}^2/\text{s}$ and $0.26 \text{cm}^2/\text{s}$ a length of 0.89mm and 0.91mm respectively. These results show the complexity of the phenomenon. Maximums and minimums in the temperature amplitude do not occur on positions where the difference in path lengths equals m respectively $(m+1/2)$ times the thermal wavelength $\lambda_{th} = 2\pi\mu_s$ (m is an integer) [13]. Instead the constant exchange of heat at the boundary between the layers influences the process continuously resulting in an amplitude of the surface temperature as can be seen in figure 5.9.

6. Discussion

In this chapter first the used setup is reviewed as far as it concerns its two main sources of inaccuracies. In 6.1 the impact of the vibrations and the particularities of the detector are reviewed.

Hereafter in 6.2 the theoretical model and the experiments are compared and its use is placed into a context.

6.1. Setup review

Two aspects are reviewed in this paragraph. First in 6.1.1 a closer look is taken at the influence of vibrations on the deflection signal. This is the major source of inaccuracy in the setup. Hereafter the problems and specific aspects of the used detector are reviewed in 6.1.2.

6.1.1. Vibrations

To gain insight in the influence of vibrations on the deflection signal the thermal wavelength is used. A change Δx in position of the probe beam relatively to the sample gives a phase difference

$$\Delta\psi = \frac{\Delta x}{\lambda_{th}} \cdot 2\pi, \quad (6.1)$$

with the sample thermal wavelength $\lambda_{th}(\text{sample}) = 5.7\text{mm}$ for the vibrations parallel to the sample surface and the fluid thermal wavelength $\lambda_{th}(\text{CCl}_4) = 0.30\text{mm}$ for directions normal to the sample surface.

As can be seen the setup is most vulnerable to the vibrations in the direction normal to the sample surface. More specifically to have an accuracy of $\pm 1^\circ$ the amplitude of the vibration should be less than $1\mu\text{m}$. This calculation shows the sensitivity of the setup to small changes of the position of the probe beam.

In practice measurements have to be taken with a setup that is as vibration-free as possible (see 3.2). Besides that measurements have to be taken at times when the sources of vibrations are minimalized, preferably at nighttime.

6.1.2. Fibre-based detector

As stated above the detector is direction insensitive, i.e. it can not distinguish between the transverse and normal component of the signal. As a result only the total deflection signal is measured. As the normal deflection is much larger than the transverse deflection (as can be seen in a calculation of (2.13) and (2.14) as well as in the actual setup in which the deflection signal goes predominantly up and down) the total deflection is assumed to be equal to the normal deflection.

This assumption has to be made considering the direction insensitivity of the detector and the impossibility to distinguish between the two components. In this context it should be noted that the detector measures the change in (probe) beam intensity, not the actual deflection. As a result the signal depends on the slope of the beam intensity profile. As this slope can be different in different directions, it is impossible to decompose the total deflection signal (for example with Pythagoras' theorem).

Regarding this it is impossible to measure the absolute deflection, the amplitude. As a result all measurements with this fibre based detector have to be phase-measurements. These kind of measurements are used throughout this report.

A specific problem resulting from the dependency of the signal on the position of the probe beam spot arises when the upward (and downward) motion of the probe beam spot induces firstly an increase in intensity on the fibre tip and secondly a decrease. This is the case when

the intensity maximum of the probe beam spot is positioned beneath the fibre tip. When deflection takes place, the maximum moves over the fibre tip, resulting in the increase followed by the decrease in intensity. In effect the signal as detected by the lock-in has a frequency of a factor two higher. This results in problems with locking on the frequency. In the setup the probe beam spot is positioned with its maximum over the fibre tip of the detector to overcome this problem. To keep this position correct the probe beam should not be moved, as discussed in 2.3. Disadvantage of this positioning is the fact that the slope of a Gaussian shaped curve, as is the case in the intensity distribution of the probe beam spot, is minimal around its center. This results in very weak signals when the deflection becomes small.

In 5.3.3 the effect of the finite value of the parameters a and z_0 was tested quantitatively. As b , the probe beam diameter, was not part of the model, its effect could not be tested. Generally the finite value of b has no effect on the temperature distribution but the signal as detected by the detector should be reviewed with care in this context. Different parts of the beam diameter oscillate with different phases when the heat wave passes through the probed area above the sample.

6.2. Experiments versus model

This paragraph aims to give an overview of the discrepancies between the practical results and the developed theoretical model. Hereafter a global conclusion concerning the research done is given.

Possible sources of discrepancies between the results as obtained with the used setup (chapter 3) and the developed theoretical model (chapter 5) are the following.

- In the model the convective and radiative heat transfer effects are neglected (see 2.2). In a (solid) GaAs sample the convective effects can be neglected, but care should be taken with the radiative effects. The model does not take the excitations into account, nor the lifetime. With a bandgap of the sample of $E_g=1.35\text{eV}$ the used pump beam ($\lambda=488\text{nm}$) can cause excitations. There are possibilities of measuring these effects, but a far more accurate setup is needed. This is not the aim of this report.
- Another assumption is that a layer in the sample is thermally and elastically isotropic. Given the crystalline structure of GaAs this is not the case.
- Another problem concerning the structure is the boundary between the layers. Where the model for the bulk sample only has boundaries between low and high thermal diffusivity layers, the model for a two-layer sample has a boundary between two high diffusivity layers. As a result the effects of this boundary on the travelling heat waves is bigger. In the particular case of this report the two layers are epitaxial.
- In the model the coupling fluid and backing are assumed to extend to infinity. Also they are assumed to be non-absorbing. The deliberately chosen coupling fluid CCl_4 has the correct characteristics. The backing however and its unknown thermal characteristics are not optimized. Although the contribution of the backing will be far less than that of the coupling fluid, its thermal characteristics can make a difference; figure 5.8 shows the evident effect of a (backing) layer on the Mirage signal.
- A last general remark is the fact that the model encompasses a lot of parameters. For an accurate comparison between the model and the practical results all these parameters should be correct.

Concluding it can be said that the model only gives a macroscopic insight in the processes that occur. The main reason for this is that the model is based on macroscopic assumptions. Microscopic effects on the scale of the individual atoms/molecules are neglected. The main question of course is whether the model can be used in combination with the Mirage setup to determine the thermal diffusivity of the layers in a two-layer sample. Theoretically this is possible under the specific condition that the diffusivity of the top layer is

larger than that of the substrate. In this case there is a theoretical straight slope (figure 5.8) with which the value of the thermal diffusivity of the substrate layer can be determined. A more practical situation arises when the thermal diffusivity of the substrate layer is known (which is practically possible by measuring it without a second layer). Then a comparison can be made between the theoretical plots (chapter 5) and the experimentally found Mirage signal. Practically with the used setup it is not possible to gain any quantitative results by comparing the theory and the practical results due to the reasons given above.

The main gains of the research are perhaps found by valuing the experimental results and the theoretical results in their own way. The experimental results offer the opportunity to gain insight in the reaction of the sample as a whole on the temperature disturbances whereas the theoretical results are a step towards understanding a particular part of the whole process.

References

- [1] Sell, J.A. (edited by), *Photothermal Investigations of Solids and Fluids* (1989).
- [2] Boccara, A.C., Fournier, D. and Badoz, J., *Appl. Phys. Lett.* **36**, 130 (1980).
- [3] Salazar, A., Sánchez-Lavega, A. and Fernández, J., *J. Appl. Phys.* **65**, 4150 (1989).
- [4] Murphy, J.C. and Aamodt, L.C., *J. Appl. Phys.* **51**, 4580 (1980).
- [5] Aamodt, L.C. and Murphy, J.C., *J. Appl. Phys.* **52**, 4903 (1981).
- [6] Salazar, A. and Sánchez-Lavega, A., *Rev. Sci. Instrum.* **65**, 2896 (1994).
- [7] Glazov, A. and Muratkov, K., *Opt. Commun.* **84**, 283 (1991).
- [8] Bertolotti, M., Li Voti, R., Liakhou, G. and Sibilica, C., *Rev. Sci. Instrum.* **64**, 1576 (1993).
- [9] Lepoutre, F., Bein, B.K., Inglehart, L.J., *Can. J. Phys.* **64**, 1037 (1986).
- [10] Chow, H.C., *J. Appl. Phys.* **51**, 4053 (1980).
- [11] Kuo et al., *Can. J. Phys.* **64**, 1165 (1986).
- [12] Hu, H., Wang, X. and Xu, X., *J. Appl. Phys.* **86**, 3953 (1999).
- [13] Suber et al., *J. Therm. Anal.* **32**, 1039 (1987).
- [14] <http://www.chem.usu.edu/faculty/SBialkow/Research/Tablevalues.html>

Appendices

A. Temperature equations

The set of equations defined by (2.6)-(2.10) can be solved [3] to obtain the temperature distribution. The solutions are:

$$T_f(r, z, t) = \frac{1}{2} \int_0^{\infty} \delta J_0(\delta r) E(\delta) \exp(-\beta_f z) \exp(i\omega t) d\delta, \quad (\text{A.1})$$

$$T_s(r, z, t) = \frac{1}{2} \int_0^{\infty} \delta J_0(\delta r) [\Gamma(\delta) \exp(\alpha z) + A(\delta) \exp(\beta_s z) + B(\delta) \exp(-\beta_s z)] \exp(i\omega t) d\delta, \quad (\text{A.2})$$

$$T_b(r, z, t) = \frac{1}{2} \int_0^{\infty} \delta J_0(\delta r) D(\delta) \exp(\beta_b(l+z)) \exp(i\omega t) d\delta, \quad (\text{A.3})$$

where $\beta_i^2 = \delta^2 + (i\omega/D_i)$, with $i=f,s,b$ and J_0 is the Bessel function of zero order. The functions of δ are given by

$$\Gamma(\delta) = \frac{P_0 \alpha}{2\pi k_s (\beta_s^2 - \alpha^2)} \exp\left(-\frac{(\delta \alpha)^2}{4}\right), \quad (\text{A.4})$$

$$A(\delta) = -\frac{\Gamma(\delta)}{H(\delta)} [(1-g)(b-p) \exp(-\alpha l) + (1+b)(g+p) \exp(\beta_s l)], \quad (\text{A.5})$$

$$B(\delta) = -\frac{\Gamma(\delta)}{H(\delta)} [(1+g)(b-p) \exp(-\alpha l) + (1-b)(g+p) \exp(-\beta_s l)], \quad (\text{A.6})$$

$$D(\delta) = \Gamma(\delta) \exp(-\alpha l) + A(\delta) \exp(-\beta_s l) + B(\delta) \exp(\beta_s l), \quad (\text{A.7})$$

$$E(\delta) = \Gamma(\delta) + A(\delta) + B(\delta), \quad (\text{A.8})$$

$$H(\delta) = (1+g)(1+b) \exp(\beta_s l) - (1-g)(1-b) \exp(-\beta_s l), \quad (\text{A.9})$$

with $g = k_f \beta_f / k_s \beta_s$, $b = k_b \beta_b / k_s \beta_s$ and $p = \alpha / \beta_s$.

B. Matlab source code

A Matlab program is used for making the calculations of the theoretical model from Chapter 5. The Matlab version used is 5.3.0.10183 (R11). The Matlab source code for calculating the integrals (5.16) – (5.18) is stated below. The function Bertolotti_2layer is used for calculating the integrals with the functions Bertolotti_2layer_temperature, Bertolotti_2layer_normal and Bertolotti_2layer_transverse to define the functions inside the integrals (5.16) – (5.18) respectively as required by the Matlab syntax. The italic source code is optional and can be varied or omitted.

```
function T_s = Bertolotti_2layer
```

```
% Used for a 2-layer sample.
% Calculates T_fluid, when all layer-parameters are known
% 'input' is a matrix with every row representing the parameters
% of a layer:
%
% l      alfa  D      k
%
% where l=thickness layer, alfa=absorption, D=thermal diffusivity and
```

```

% k=thermal conductivity all in SI units (m,K,s,kg)
% Row number n (index): 1: fluid; 2: top layer; 3: bulk semiconductor
% and 4: backing

global input;          % input parameters material
global n_max;         % number of layers in system
global n;             % layer number
global f;             % pump beam chopping frequency
global a;             % pump beam diameter
global z;             % probe beam height
global y;             % pump/probe separation

% use 'input' for setting the input parameters

%
input = [ 1      alfa      D      k
         inf     0         2e-7   0.1;    % fluid
         6e-6    1e2       26e-6   56;     % top layer
         400e-6  1e2       25e-6   56;     % bulk layer
         inf     0         2e-7   0.1];    % backing layer

% calculate k1 for equal density and heat capacity in both layers
input(2,4) = input(3,4).*input(2,3)./input(3,3);
% calculate k2 for equal density and heat capacity in both layers
input(3,4) = input(2,4).*input(3,3)./input(2,3);

n_max = 4;
f = 10;
a = 600e-6;
z = 100e-6;

% Calculate the normal and transverse deflection
ytot = 0:0.0001:0.003;
for n = 1:length(ytot)
    y = ytot(n);
    Temp(n) = quad8('Bertolotti_2layer_temperature',0,100000);
    Phi_n(n) = quad8('Bertolotti_2layer_normal',0,100000);
    Phi_t(n) = quad8('Bertolotti_2layer_transverse',0,100000);
end

plot(ytot,Temp);
plot(ytot,Phi_n);
plot(ytot,Phi_t);

% Phase plot Phi_t; accounts for the fact that the function 'angle'
% only ranges between -pi and pi radians.
Phi_t = angle(Phi_t);
for n0 = 2:length(ytot)
    if (Phi_t(n0-1)-Phi_t(n0)) > 5
        Phi_t(n0:length(ytot)) = Phi_t(n0:length(ytot)) + 2.*pi;
    elseif (Phi_t(n0)-Phi_t(n0-1)) > 5
        Phi_t(n0:length(ytot)) = Phi_t(n0:length(ytot)) - 2.*pi;
    end
end
end

```

In the above program, the functions used in the integrals have to be defined separately by Matlab functions. These are as follows:

```

function T_s = Bertolotti_2layer_temperature(delta)
    Bertolotti_2layer_normal(delta)
    Bertolotti_2layer_transverse(delta)

global input;          % input parameters material
global n_max;         % number of layers in system
global n;             % layer number
global f;             % pump beam chopping frequency
global a;             % pump beam diameter
global z;             % probe beam height
global y;             % pump/probe separation

l1 = input(2,1);      % thickness first layer
l2 = input(2,1)+input(3,1); % thickness first two layers

alf1 = input(2,2);    % alf0 and alf3 assumed 0
alf2 = input(3,2);

k0 = input(1,4);
k1 = input(2,4);
k2 = input(3,4);
k3 = input(4,4);

beta = sqrt(ones(n_max,1)*delta.^2+(i*f*2*pi)./(input(:,3))*...
    (ones(1,length(delta))));
beta0 = beta(1,:);
beta1 = beta(2,:);
beta2 = beta(3,:);
beta3 = beta(4,:);

E1_0 = alf1.*exp(-(a.*delta).^2./8)./(k1.*(beta1.^2-alf1.^2));
E1_l1 = alf1.*exp(-(a.*delta).^2./8-alf1.*l1)./...
    (k1.*(beta1.^2-alf1.^2));
E2_l1 = alf2.*exp(-(a.*delta).^2./8-alf2.*l1-l1.*(alf1-alf2))./...
    (k2.*(beta2.^2-alf2.^2));
E2_l2 = alf2.*exp(-(a.*delta).^2./8-alf2.*l2-l1.*(alf1-alf2))./...
    (k2.*(beta2.^2-alf2.^2));

c1 = (beta0*k0)./(beta1.*k1);
c2 = (beta1*k1)./(beta2.*k2);
c3 = (beta2*k2)./(beta3.*k3);
c33 = (1+c3)./(1-c3);

% T_s = -([2]-[3]*[1])/(1+k0*beta0*[1])

% [1] = U1/U2
U1 = (1+c2).*exp(-2.*(beta1.*l1+beta2.*(l2-l1)))+(c2-1).*...
    exp(-2.*beta1.*l1).*c33-(1-c2).*exp(-2.*beta2.*(l2-l1))+...
    (1+c2).*c33;
U2 = k1.*beta1.*((1+c2).*exp(-2.*(beta1.*l1+beta2.*(l2-l1)))+...
    (c2-1).*exp(-2.*beta1.*l1).*c33+(1-c2).*exp(-2.*beta2.*...
    (l2-l1)))-(1+c2).*c33;

% [2] = -E1_0+V1/V2
V1 = E1_l1.*(exp(-2.*beta2.*(l2-l1))-c33+(k1.*alf1)./(k2.*beta2).*...
    (exp(-2.*beta2.*(l2-l1))+c33))-E2_l1.*(exp(-2.*beta2.*(l2-l1))-...
    c33+(k2.*alf2)./(k2.*beta2).*(exp(-2.*beta2.*(l2-l1))+c33))+...
    E2_l2.*exp(-2.*beta2.*l2+beta2.*l1).*2.*(1-(k2.*alf2)./...
    (k3.*beta3))./(1-c3);
V2 = exp(-beta1.*l1).*(exp(-2.*beta2.*(l2-l1))-c33+c2.*...
    (exp(-2.*beta2.*(l2-l1))+c33));

```

```

% [3] = -E1_0*k1*alf1 + k1*beta1(V1/V2)

% Terms rearranged to avoid singularities
% For Bertolotti_2layer_temperature(delta)
T_s = besselj(0,delta.*y).*((E1_0-V1./V2-(E1_0.*k1.*alf1-
k1.*beta1.*...
(V1./V2)).*(U1./U2))./(1+k0.*beta0.*(U1./U2))).*...
exp(-beta0.*z).*delta;

% For Bertolotti_2layer_normal(delta)
T_s = cos(delta.*y).*((E1_0-V1./V2-(E1_0.*k1.*alf1-k1.*beta1.*...
(V1./V2)).*(U1./U2))./(1+k0.*beta0.*(U1./U2))).*...
exp(-beta0.*z).*beta0;

% For Bertolotti_2layer_transverse(delta)
T_s = sin(delta.*y).*((E1_0-V1./V2-(E1_0.*k1.*alf1-k1.*beta1.*...
(V1./V2)).*(U1./U2))./(1+k0.*beta0.*(U1./U2))).*...
exp(-beta0.*z).*delta;

```

Acknowledgements

Komt nog!